

NASA TN D-951

NASA TN D-951



IN-02
380-526

TECHNICAL NOTE

D-951

SUPERSONIC FREE-FLIGHT MEASUREMENT OF HEAT TRANSFER
AND TRANSITION ON A 10° CONE HAVING A
LOW TEMPERATURE RATIO

By Charles F. Merlet and Charles B. Rumsey

Langley Research Center
Langley Field, Va.

NATIONAL AERONAUTICS AND SPACE ADMINISTRATION
WASHINGTON

August 1961

•

•

•

•

•

•

L
NATIONAL AERONAUTICS AND SPACE ADMINISTRATION

TECHNICAL NOTE D-951

SUPERSONIC FREE-FLIGHT MEASUREMENT OF HEAT TRANSFER
AND TRANSITION ON A 10° CONE HAVING A
LOW TEMPERATURE RATIO¹

By Charles F. Merlet and Charles B. Rumsey

L
1
7
0
0
SUMMARY

Heat-transfer coefficients in the form of Stanton number and boundary-layer transition data were obtained from a free-flight test of a 100-inch-long 10° total-angle cone with a 1/16-inch tip radius which penetrated deep into the region of infinite stability of laminar boundary layer over a range of wall-to-local-stream temperature ratios and for local Mach numbers from 1.8 to 3.5. Experimental heat-transfer coefficients, obtained at Reynolds numbers up to 160×10^6 , were in general somewhat higher than theoretical values. A maximum Reynolds number of transition of only 33×10^6 was obtained. Contrary to theoretical and some other experimental investigations, the transition Reynolds number initially increased while the wall temperature ratio increased at relatively constant Mach number. Further increases in wall temperature ratio were accompanied by a decrease in transition Reynolds number. Increasing transition Reynolds number with increasing Mach number was also indicated at a relatively constant wall temperature ratio.

INTRODUCTION

The Pilotless Aircraft Research Division of the Langley Aeronautical Laboratory is currently conducting a program to measure the aerodynamic heating and Reynolds number for boundary-layer transition on bodies in free flight at high Mach numbers. Data of this type are reported in reference 1 for a 10° total-angle cone, 40 inches in length, over a Mach number range from 1.15 to 3.7. The present test was also conducted with a 10° total-angle cone, and was planned to extend the results of reference 1 by obtaining test conditions deeper within the region of two-dimensional infinite laminar-boundary-layer stability defined by reference 2. In order to obtain low wall-to-stream temperature ratios, the

¹Supersedes the recently declassified NACA Research Memorandum L56L10, by Charles F. Merlet and Charles B. Rumsey, 1957.

model skin was made of thick copper, selected because of its high heat capacity and thermal diffusivity. In order to measure large transition Reynolds numbers in the event they should occur, the nose cone was made 100 inches long, providing test Reynolds numbers up to 160×10^6 .

Although test conditions were obtained well into the region of two-dimensional stability, turbulent heating at all measurement stations during the early part of the test resulted in higher than anticipated wall-to-stream temperature ratios and the test conditions were only slightly deeper within the stability region than those of reference 1.

The measurements of transition Reynolds number and local heat-transfer coefficient are presented for a Mach number range of 1.8 to 3.5 and for a range of Reynolds numbers from 5×10^6 to 164×10^6 based on nose length to a measurement station. The flight test was performed at the Langley Pilotless Aircraft Research Station at Wallops Island, Va.

SYMBOLS

A	area, sq ft
c_f	local skin-friction coefficient
c_p	specific heat of air at constant pressure, Btu/lb-°F
c_w	specific heat of wall material, Btu/lb-°F
g	acceleration due to gravity, 32.2 ft/sec ²
h	local aerodynamic heat-transfer coefficient, Btu/sec-ft ² -°F
k	thermal conductivity of air, Btu-ft/sec-°F-ft ²
k_w	thermal conductivity of wall material, Btu-ft/sec-°F-ft ²
M	Mach number
N_{Pr}	Prandtl number, $gc_p\mu/k$
N_{St}	Stanton number, $\frac{h}{g\rho_v c_p V_v}$

Q	quantity of heat, Btu
R	Reynolds number, $\rho Vx/\mu$
T	absolute temperature, $^{\circ}R$
t	time, sec
V	velocity, ft/sec
x	axial distance, ft, unless otherwise noted
ϵ	emissivity
μ	absolute viscosity of air, slugs/ft-sec
ρ	density of air, slugs/cu ft
ρ_w	density of wall material, lb/cu ft
σ	Stefan-Boltzmann constant, 0.4806×10^{-12} , Btu/ft ² -sec-($^{\circ}R$) ⁴
τ	skin thickness, ft

Subscripts:

aw	adiabatic wall
s	stagnation
tr	at transition point
v	local condition just outside boundary layer
w	at wall

MODEL, INSTRUMENTATION, AND TESTS

Model

The model was a 100-inch long cone having a total angle of 10° , mounted on an M5 Jato rocket motor as shown in figures 1 and 2. The complete configuration was stabilized by four fins. Except for the

tip, the cone was constructed from two conic sections joined by a circumferential weld at station 58.5 (that is, 58.5 inches from the nose tip). These sections were formed from two copper sheets of which the thicknesses were 0.077 and 0.080 \pm 0.002 inch. The thinner sheet formed the skin ahead of station 58.5. The weld was done with a copper rod of the same composition as the sheet. The model tip, made of steel, was welded to the first conic section at station 6. The sharp point was blunted with a small radius (approximately 1/16 inch) to prevent excessive heating. After construction was completed, the exterior surface of the cone was polished. Random sample measurements of the surface roughness as determined by a Physicists Research Company Profilometer varied from 10 to 16 microinches rms. However, subsequent to the flight test, sample roughness measurements made with the Profilometer were checked optically with a fringe-type interference microscope. The average roughness measured optically was about 8 to 10 times the root-mean-square value read on the Profilometer for a copper sample. Also, discrete scratches were observed optically which apparently did not influence the profilometer measurements. It appears that the average surface roughness of the model skin may have been of the order of 100 to 150 microinches.

L-1700

Instrumentation

The model was equipped with 12 thermocouples located in line axially along the cone from station 12 to 88 as indicated in figure 1. The thermocouples, made from no. 30 chromel-alumel wire, were installed by drilling separate holes for each wire approximately 1/4 inch apart and soldering the wires in place with high-temperature silver solder. The external surface was then polished.

The 12 thermocouple outputs were commutated and transmitted on two telemeter channels. Each channel transmitted six thermocouple outputs and three standard voltages at a rate of 14 times per second and 7 times per second, respectively. The standard voltages chosen were equivalent to the lowest, middle, and highest temperatures expected and served as an in-flight calibration of the telemeter throughout the flight.

Test

The model was launched at an elevation angle of 70° (fig. 2) and propelled to a maximum flight Mach number of 3.6 by a single M5 Jato booster rocket motor. Data were obtained during the accelerating portion of the flight and the decelerating portion subsequent to rocket-motor burnout. Flight velocity was determined from CW Doppler radar. Altitude and flight-path data were obtained from measurements made by an NACA modified SCR-584 tracking radar. Ambient air conditions as well as winds aloft were measured with a radiosonde used in conjunction with an AN/CMD-1A rawin set.

Figure 3 shows the time histories of flight Mach number, altitude, and free-stream Reynolds number per foot.

DATA REDUCTION

The time rate of change of heat within the skin at a given location on the conical nose can be written as follows:

$$\frac{dQ}{dt} = \rho_w c_w \tau A \frac{dT_w}{dt} = hA(T_{aw} - T_w) - A\sigma\epsilon T_w^4 + Ak_w \tau \left(\frac{\partial^2 T_w}{\partial x^2} + \frac{1}{x} \frac{\partial T_w}{\partial x} \right) \quad (1)$$

The three terms on the right-hand side of equation (1) account for the aerodynamic heat transfer to the skin, the radiation of heat from the skin externally, and the rate of heat conduction along the skin, respectively. This equation neglects the heat absorbed by the skin from solar radiation and heat radiated inward from the skin, which are compensating and estimated to be negligible.

In the data presented herein, the effects of conduction along the skin have been neglected since calculations indicated that the largest conduction effects were less than 2 percent of the aerodynamic heat transfer. Radiation effects have not been included because the value of emissivity for copper varies greatly with surface conditions, and the effects on the surface condition of flight test conditions of temperature and velocity are unknown. Radiation effects were checked, however, using an emissivity of 0.70, which is for heavily oxidized copper, and the highest value reported. The radiation effects thus calculated in general amounted to 10 percent or less of the aerodynamic heating from 10 seconds on. At earlier times, radiation in general was less than 5 percent of the aerodynamic heating. In no case, however, could the radiation effects alter the heat-transfer data sufficiently to influence the determination of the location of boundary-layer transition.

The adiabatic wall temperature T_{aw} was calculated from local stream conditions outside the boundary layer as determined from reference 3, using a recovery factor of $N_{Pr}^{1/2}$ and $N_{Pr}^{1/3}$ based on local temperature for laminar and turbulent boundary layer, respectively. Stanton number was then computed as follows:

$$N_{St} = \frac{h}{g\rho_v c_p V_v}$$

RESULTS AND DISCUSSION

Skin Temperatures

The measured skin temperatures for each station are presented in table I for each time for which data have been reduced. The table also presents the corresponding local Mach number and Reynolds number per foot, and the corresponding values of $\frac{1}{A} \frac{dQ}{dt}$, the time rate of change of heat within a square foot of skin.

The temperature-time curves of the first five stations are plotted in figure 4, along with local Mach number just outside the boundary layer, as a function of time. The curves for the remaining stations are not plotted inasmuch as they would vary only slightly (see values for temperatures given in table I) from those shown for stations 27 and 35.

The abrupt decrease in slope of the temperature-time curves for stations 17 and 22 at time 3.5 and 4.0 seconds, respectively, and the earlier, more gradual reduction in slope for station 12 indicate transition from turbulent to laminar or transitional flow. However, the character of the boundary layer and the location of transition can be determined more readily from the heat-transfer coefficients, and will be discussed later.

Heat-Transfer Coefficient

The heat-transfer coefficients in the form of Stanton numbers are presented in figure 5 as a function of axial distance along the body. The wall temperature ratios are also shown, as well as the theoretical values of N_{St} . The theoretical Stanton numbers for conical laminar flow were obtained by multiplying the flat-plate values of reference 4 by $\sqrt{3}$. The theoretical turbulent values of N_{St} were obtained from c_f values by the conversion of reference 5 (that is, $N_{St} = 0.6c_f$). The values of c_f were obtained from charts of Van Driest's flat-plate theory presented in reference 6 and converted to conical flow by the method of reference 7.

In general, the experimental turbulent values are in fair agreement with theory. From 3.0 seconds on, the experimental values tend to be somewhat higher than the theoretical predictions for both laminar and turbulent values. The data at 7.0 and 10.0 seconds, which exhibited the most scatter, occurred near the peak of the temperature-time curves (see fig. 4) and therefore have low forcing functions ($T_{aw} - T_w$) and are least accurate. The remaining data, however, are unaccountably higher than theory.

Boundary-Layer Transition

The disagreement between theory and experiment is not enough to preclude the determination of transition, and the variation of transition along the cone as the flight time progressed is apparent. The experimental Stanton numbers of figure 5 indicate that prior to 3.0 seconds fully turbulent flow occurred at least as far forward as station 12, the first measuring station. Transition occurred first at the forward measuring station, then moved rearward with time until, at 4.5 seconds, station 22 showed laminar flow with a local Reynolds number of 33×10^6 . Transition then moved forward again until at 14 seconds the flow was again fully turbulent at station 12 and rearward.

The transition data determined from the data presented in figure 5 include a variation of both Mach number and wall temperature ratio. The variation of wall temperature ratio with local Mach number for the transition points (taken as the last station with a laminar heat-transfer coefficient) is shown in figure 6. The corresponding Reynolds number based on local conditions is indicated for each point in the figure. The broken curve shows for comparison the conditions of M_V and T_w/T_V of the test of reference 1. Also presented in the figure is the curve bounding the region of theoretical infinite laminar stability for two-dimensional disturbances as determined by Van Driest in reference 2. It was this region that the model was designed to explore, and it can be seen that the data penetrated well into it. A more recent paper by Dunn and Lin (ref. 8), however, indicates that an infinite stability region cannot be found for three-dimensional disturbances. However, Dunn and Lin conclude that sufficient cooling can stabilize the boundary layer to very large Reynolds numbers.

The present data are somewhat at variance with this trend, as can be seen in figure 7, where transition Reynolds number is plotted against wall temperature parameter $\frac{T_w - T_{aw}}{T_s}$. The usual trend, as indicated by the stability theory, is illustrated by the data from reference 9 which show an increase in transition Reynolds number as the wall is cooled. The data of the present test for a relatively constant Mach number (from 3.5 to 3.2), on the other hand, show an increase in Reynolds number of transition as the wall temperature increased from a temperature parameter of -0.50 to -0.31, corresponding to a wall temperature ratio change from 1.2 to 1.65. With a further decrease in temperature parameter as Mach number continued to decrease from 3.2 to 2.8, the transition Reynolds number decreased rather sharply. Although the reason for this behavior of transition Reynolds number with cooling is not known, data reported in reference 10 show that for certain degrees of roughness, cooling produces similar trends in transition Reynolds number, apparently by causing an excessive thinning of the boundary layer in comparison to the roughness.

As previously mentioned (see section entitled "Model"), the average roughness of the present copper skin may have been 100 to 150 microinches in comparison with computed boundary-layer displacement thickness at the transition station of 0.0048 inch for the coolest wall condition ($R_{tr} = 22.1 \times 10^6$) and 0.0086 inch at maximum transition Reynolds number of 33.1×10^6 .

The data of reference 1, also shown in figure 7, indicate a similar trend, in that cooling beyond a certain point showed no further increase in transition Reynolds number. The average roughness of the model of reference 1, however, is estimated to be only 10 to 20 microinches, whereas computed boundary-layer displacement thicknesses are of the same order as those of the present test. (The estimated roughness of the model in ref. 1 is based on a comparison of the roughness of an Inconel sample determined from optical and profilometer measurements which indicated the average roughness may have been 3 to 4 times the profilometer measurements of 3 to 5 microinches rms reported in ref. 1.)

The measured transition Reynolds numbers of the present test were considerably higher than those reported in reference 1 despite the larger roughness of the present model. However, since the tip of the present model was blunted to a 1/16-inch radius while the tip of reference 1 model was sharp, the difference in magnitude of transition Reynolds numbers may be due, in part at least, to the beneficial effects of tip bluntness described in reference 11. Reference 11 points out that the detached shock wave associated with the blunt tip results in a "low Mach number region" of air flowing over the body. When the body boundary layer is enveloped by this low energy air, large increases in transition Reynolds number will result. In the present case, tip bluntness of the model was not large enough to envelope completely the laminar boundary layer in the low Mach number region defined in reference 11; however, comparison of the computed boundary-layer thickness with the inviscid Mach number profiles presented in reference 11 indicated the bluntness was enough so that the inviscid Mach number at the edge of the boundary layer at transition stations was markedly reduced below theoretical cone values.

Thus it appears that the difference in magnitude of transition Reynolds number in these two tests may be due, in part at least, to the bluntness of the tip of the present model. The similarity of trend of transition Reynolds number with increased cooling, however, is still not explained completely. Apparently some factor besides roughness influenced the trend of transition Reynolds number with cooling in these tests.

The transition Reynolds numbers for the latter part of the flight are shown in figure 8 as a function of Mach number for wall temperature

ratios T_w/T_v from approximately 1.5 to 1.9. The data indicate a distinct increase in transition Reynolds number with Mach number for this model. A similar trend was noted in reference 1 for skin temperature ratios of about 1.2 to 1.3, although the Reynolds number increase was not as pronounced in reference 1. It is believed that this increased slope of transition Reynolds number with Mach number in the present test can be attributed to the effect on local Reynolds number of the tip bluntness employed on the present model. As indicated in reference 11, the effect of bluntness on local Reynolds number is greater as Mach number increases.

CONCLUDING REMARKS

Heat-transfer coefficients in the form of Stanton number and boundary-layer transition data were obtained from a free-flight test of a 10° total-angle conical nose with a 1/16-inch tip radius over a Mach number range from 1.8 to 3.5 and a range of wall-to-local-stream temperature ratios. In general, experimental heat-transfer coefficients were somewhat higher than theoretical predictions for turbulent values for Reynolds numbers up to 160×10^6 . A maximum Reynolds number of transition of 33×10^6 was obtained. Contrary to theoretical and some other experimental investigations, the Reynolds number of transition initially increased while the wall temperature ratio increased at relatively constant Mach number. Further increases in wall temperature ratio were accompanied by a decrease in transition Reynolds number. A favorable effect of increasing Mach number on transition Reynolds number was also indicated at a relatively constant wall temperature ratio.

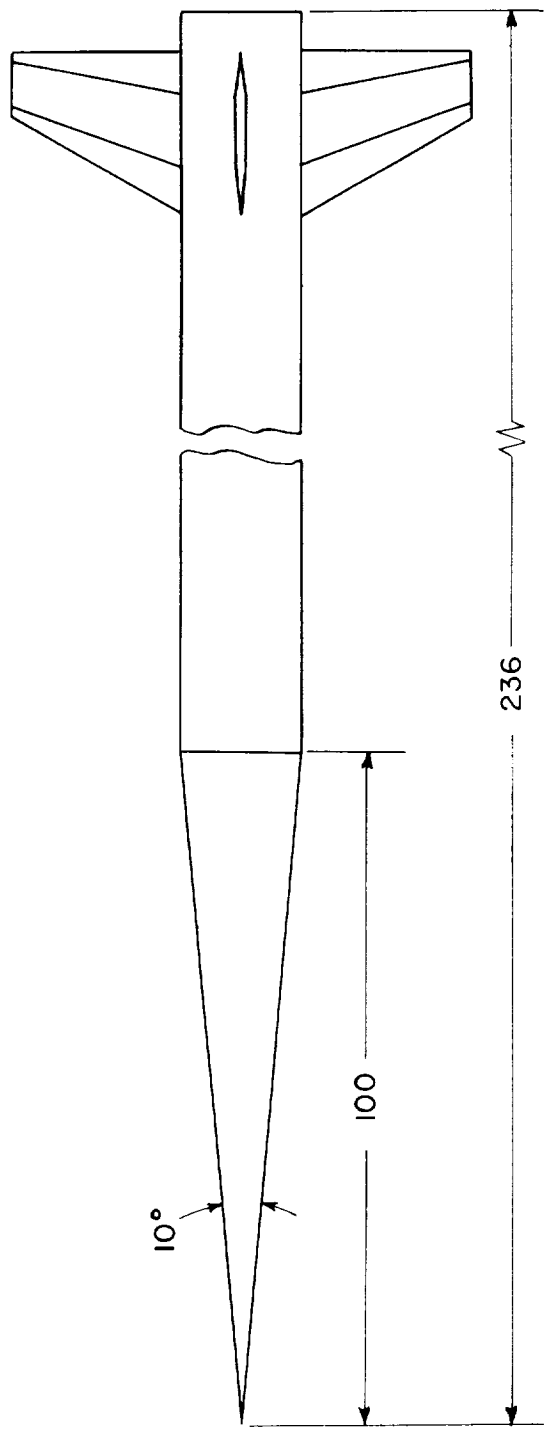
Langley Aeronautical Laboratory,
National Advisory Committee for Aeronautics,
Langley Field, Va., November 23, 1956.

REFERENCES

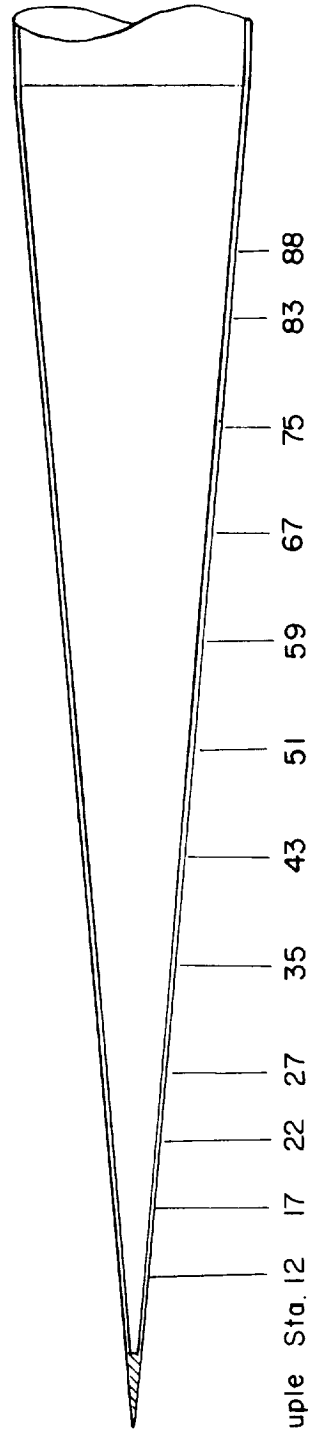
1. Rumsey, Charles B., and Lee, Dorothy B.: Measurements of Aerodynamic Heat Transfer and Boundary-Layer Transition on a 10° Cone in Free Flight at Supersonic Mach Numbers up to 5.9. NASA TN D-745, 1961. (Supersedes NACA RM L56B07.)
2. Van Driest, E. R.: Calculation of the Stability of the Laminar Boundary Layer in a Compressible Fluid on a Flat Plate With Heat Transfer. Jour. Aero. Sci., vol. 19, no. 12, Dec. 1952, pp. 801-812.
3. Staff of the Computing Section, Center of Analysis (Under Direction of Zdeněk Kopal): Tables of Supersonic Flow Around Cones. Tech. Rep. No. 1 (NOrd Contract No. 9169), M.I.T., 1947.
4. Van Driest, E. R.: Investigation of Laminar Boundary Layer in Compressible Fluids Using the Crocco Method. NACA TN 2597, 1952.
5. Rubesin, Morris W.: A Modified Reynolds Analogy for the Compressible Turbulent Boundary Layer on a Flat Plate. NACA TN 2917, 1953.
6. Lee, Dorothy B., and Faget, Maxime A.: Charts Adapted From Van Driest's Turbulent Flat-Plate Theory for Determining Values of Turbulent Aerodynamic Friction and Heat-Transfer Coefficients. NACA TN 3811, 1956.
7. Van Driest, E. R.: Turbulent Boundary Layer on a Cone in a Supersonic Flow at Zero Angle of Attack. Jour. Aero. Sci., vol. 19, no. 1, Jan. 1952, pp. 55-57, 72.
8. Dunn, D. W., and Lin, C. C.: On the Stability of the Laminar Boundary Layer in a Compressible Fluid. Jour. Aero. Sci., vol. 22, no. 7, July 1955, pp. 455-477.
9. Jack, John R., and Diaconis, N. S.: Variation of Boundary-Layer Transition With Heat Transfer on Two Bodies of Revolution at a Mach Number of 3.12. NACA TN 3562, 1955.
10. Van Driest, E. R., and Boison, J. Christopher: Research on Stability and Transition of the Laminar Boundary Layer. Technical Report Covering Experiments on a 20-Inch 10-Degree (Apex Angle) Cone in the 12-Inch Supersonic Wind Tunnel of the Jet Propulsion Laboratory. Rep. No. AL-2196 (Contract AF 18(600)-786), North American Aviation, Inc., Sept. 1955.
11. Moeckel, W. E.: Some Effects of Bluntness on Boundary-Layer Transition and Heat Transfer at Supersonic Speeds. NACA Rep. 1312, 1957. (Supersedes NACA TN 3653.)

TABLE I.- SUMMARY OF DATA.

Time, sec	M _g	R _g /ft	Station 12		Station 17		Station 22		Station 27		Station 33		Station 43		Station 51		Station 59		Station 67		Station 75		Station 83		Station 88			
			T _w , °R	T _g , °R	$\frac{1}{A} \frac{dQ}{dt}$, Btu ft ² -sec	$\frac{1}{A} \frac{dQ}{dt}$, A ft ²	T _w , °R	T _g , °R	$\frac{1}{A} \frac{dQ}{dt}$, Btu ft ² -sec	$\frac{1}{A} \frac{dQ}{dt}$, A ft ²	T _w , °R	T _g , °R	$\frac{1}{A} \frac{dQ}{dt}$, Btu ft ² -sec	$\frac{1}{A} \frac{dQ}{dt}$, A ft ²	T _w , °R	T _g , °R	$\frac{1}{A} \frac{dQ}{dt}$, Btu ft ² -sec	$\frac{1}{A} \frac{dQ}{dt}$, A ft ²	T _w , °R	T _g , °R	$\frac{1}{A} \frac{dQ}{dt}$, Btu ft ² -sec	$\frac{1}{A} \frac{dQ}{dt}$, A ft ²	T _w , °R	T _g , °R	$\frac{1}{A} \frac{dQ}{dt}$, Btu ft ² -sec	$\frac{1}{A} \frac{dQ}{dt}$, A ft ²	T _w , °R	T _g , °R
2.0	1.15	13.5 × 10 ⁻⁵	538	563	20.9	563	17.0	565	17.5	562	15.2	563	18.3	560	15.5	563	16.2	560	14.5	563	18.9	563	15.5	563	18.9	563	18.9	563
2.5	2.04	18.2	542	607	33.1	604	34.4	601	37.6	594	34.8	595	29.4	590	31.1	596	34.2	592	28.8	592	29.5	592	29.9	592	29.5	592	29.5	592
3.0	3.23	22.1	550	650	51.4	667	56.3	676	60.8	666	59.1	663	62.3	658	55.3	665	61.4	651	53.2	651	50.0	650	56.3	649	56.3	656	59.2	656
3.5	3.48	22.4	547	684	20.3	768	43.9	772	61.1	757	62.1	755	58.3	745	57.5	760	63.0	736	57.4	736	56.3	735	57.4	735	56.3	735	56.3	735
4.0	3.31	20.2	556	711	17.3	812	28.3	852	48.6	837	42.0	829	44.6	880	33.9	836	43.5	810	42.6	810	42.6	810	42.6	810	42.6	810	42.6	810
4.5	3.15	18.1	527	732	11.6	824	8.0	905	26.0	883	26.2	877	29.3	865	25.6	885	27.0	856	27.2	856	27.2	856	27.2	856	27.2	856	27.2	856
5.0	3.01	16.3	521	747	10.8	833	10.3	934	18.8	822	13.8	908	13.4	876	20.1	917	18.8	885	13.0	885	13.0	885	13.0	885	13.0	885	13.0	885
6.0	2.78	15.5	508	775	7.2	848	5.2	967	5.4	957	8.5	950	9.4	936	9.1	954	8.5	923	9.5	923	9.5	923	9.5	923	9.5	923	9.5	923
7.0	2.58	11.3	498	791	4.5	863	3.3	975	2.1	972	1.7	966	4.5	953	4.0	966	2.8	941	3.2	941	3.2	941	3.2	941	3.2	941	3.2	941
10.0	2.17	7.5	462	816	1.6	885	-2.3	960	-2.9	965	-3.2	959	-1.8	950	-2.4	959	-2.7	959	-2.5	959	-2.5	959	-2.5	959	-2.5	959	-2.5	959
12.0	1.96	6.1	440	818	-0.3	872	-2.4	909	-5.3	943	-4.2	941	-1.5	930	-5.1	937	-4.6	922	-5.3	922	-5.3	922	-5.3	922	-5.3	922	-5.3	922
14.0	1.79	5.0	421	815	-2.6	854	-4.2	910	-4.5	918	-4.2	916	-4.2	910	-5.5	912	-3.6	903	-3.6	903	-3.6	903	-3.6	903	-3.6	903	-3.6	903



Station 0



Thermocouple Sta. 12 17 22 27 35 43 51 59 67 75 83 88

Figure 1.- General configuration. All dimensions are in inches.

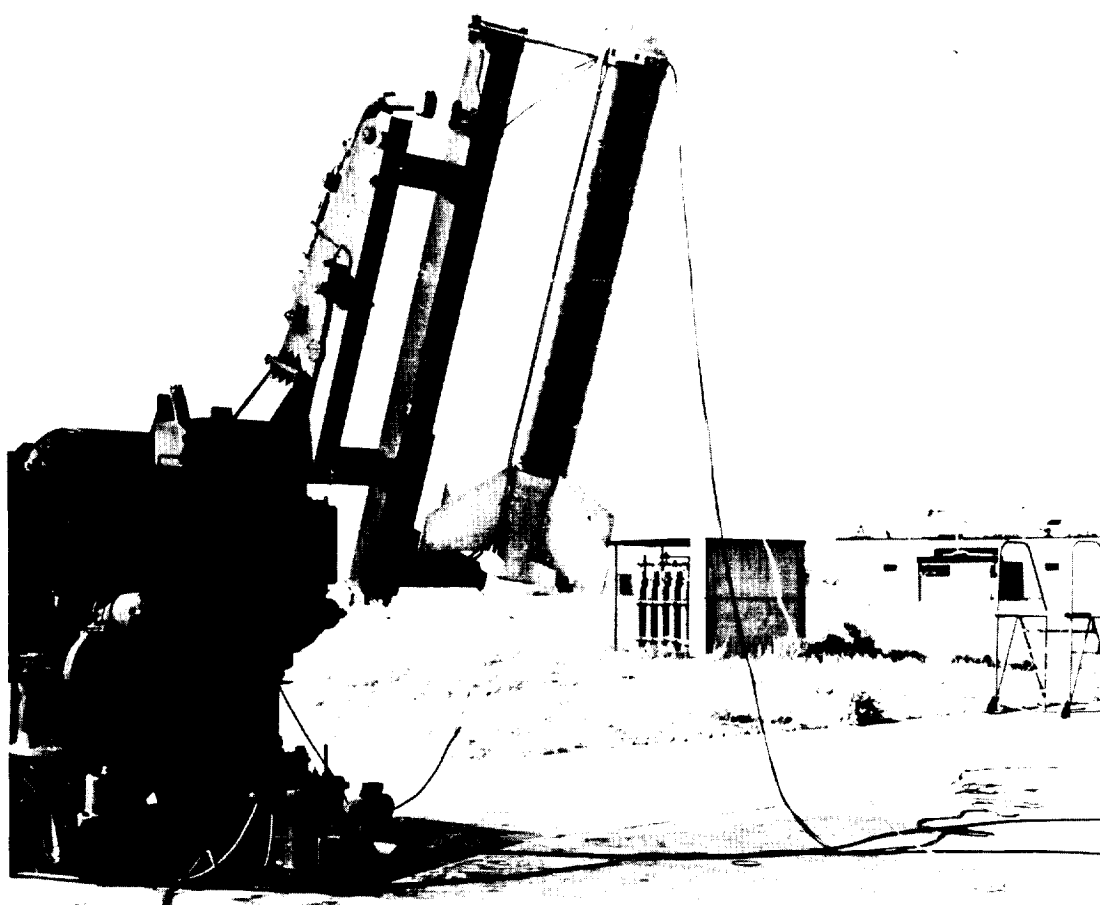


Figure 2.- Model on the launcher.

L-89648.1

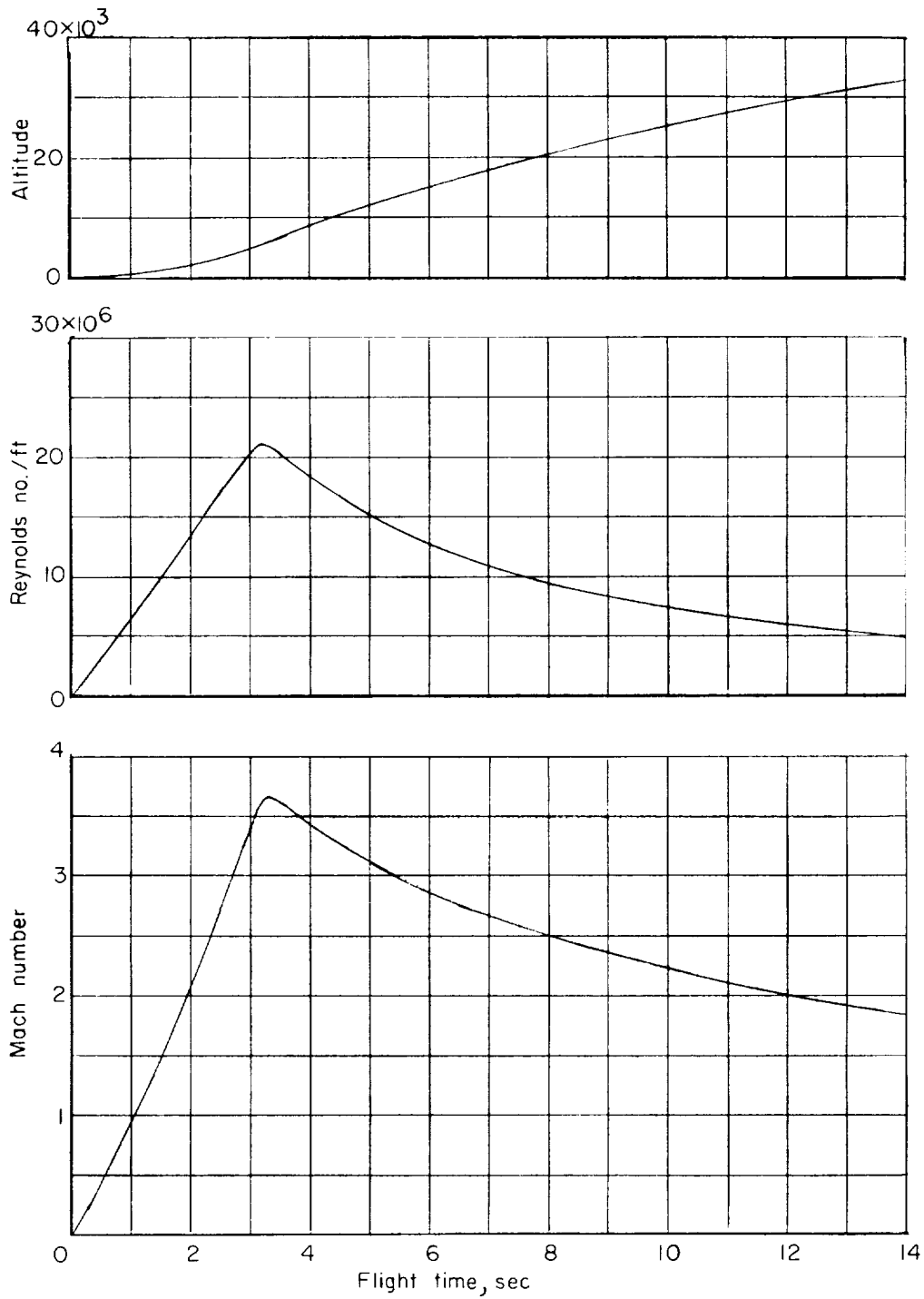


Figure 3.- Time histories of free-stream Mach number, Reynolds number per foot, and altitude.

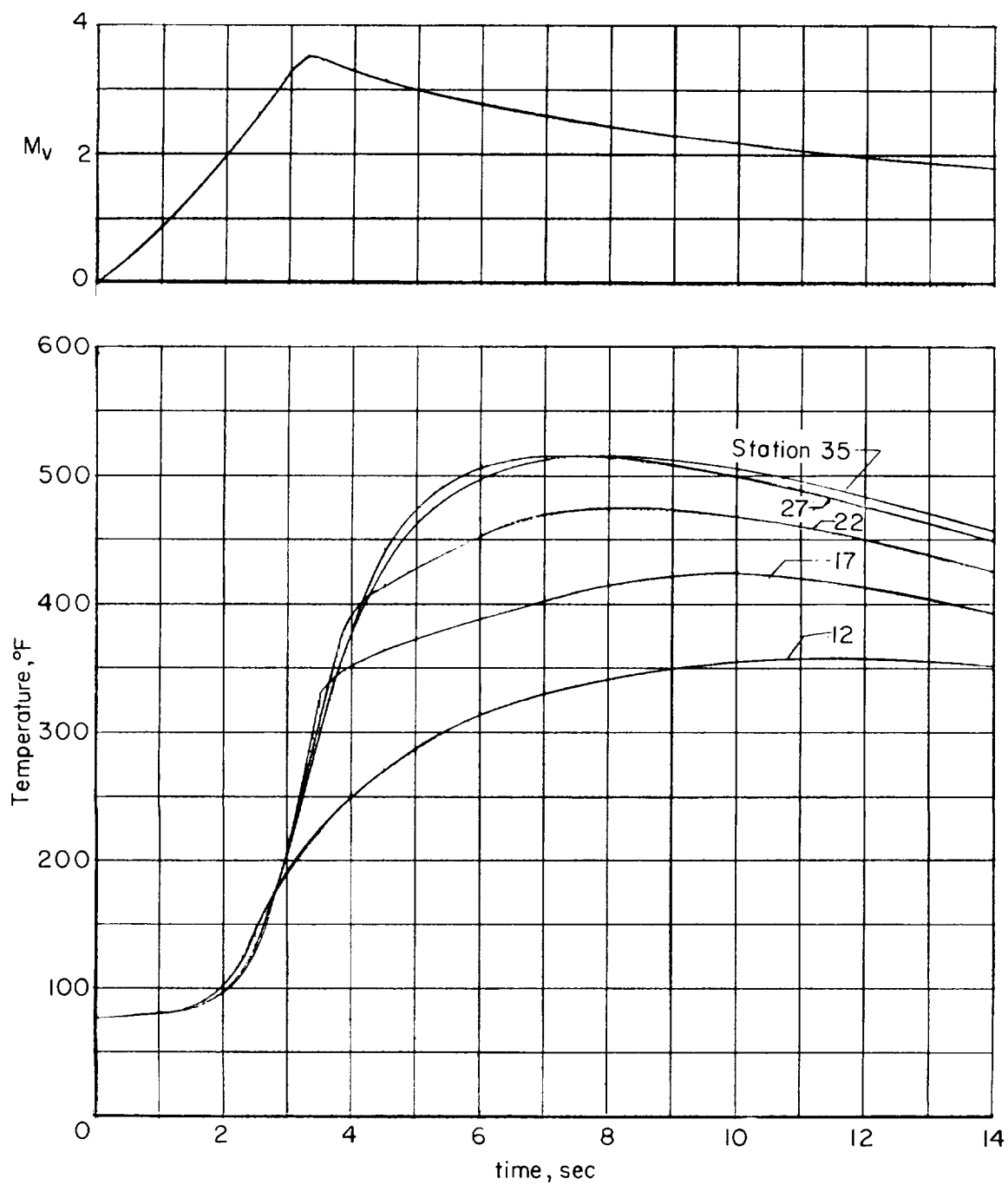
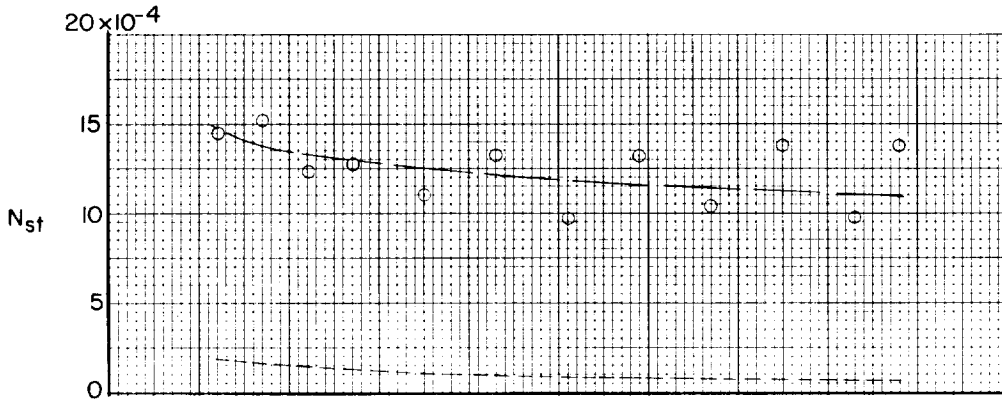
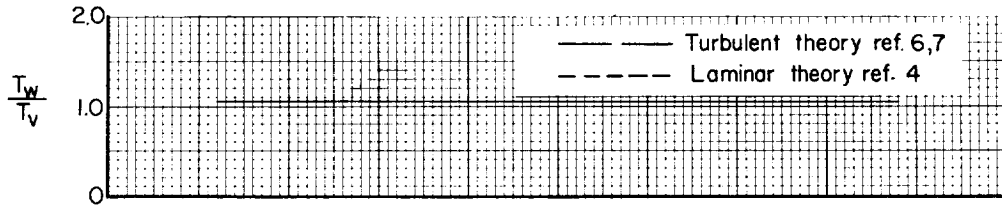
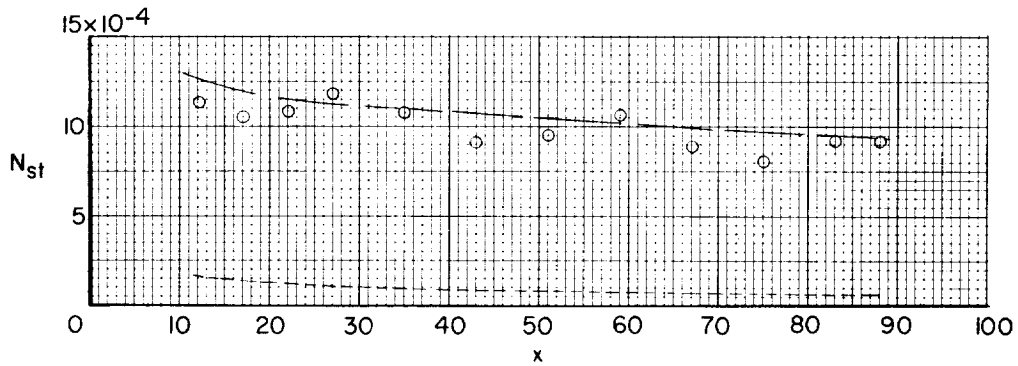
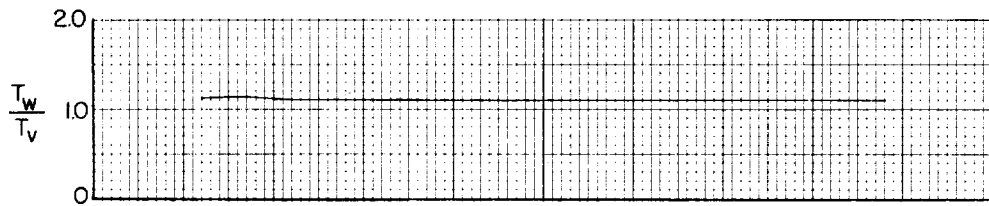


Figure 4.- Time histories of the local Mach number just outside boundary layer and the temperatures measured at various stations.

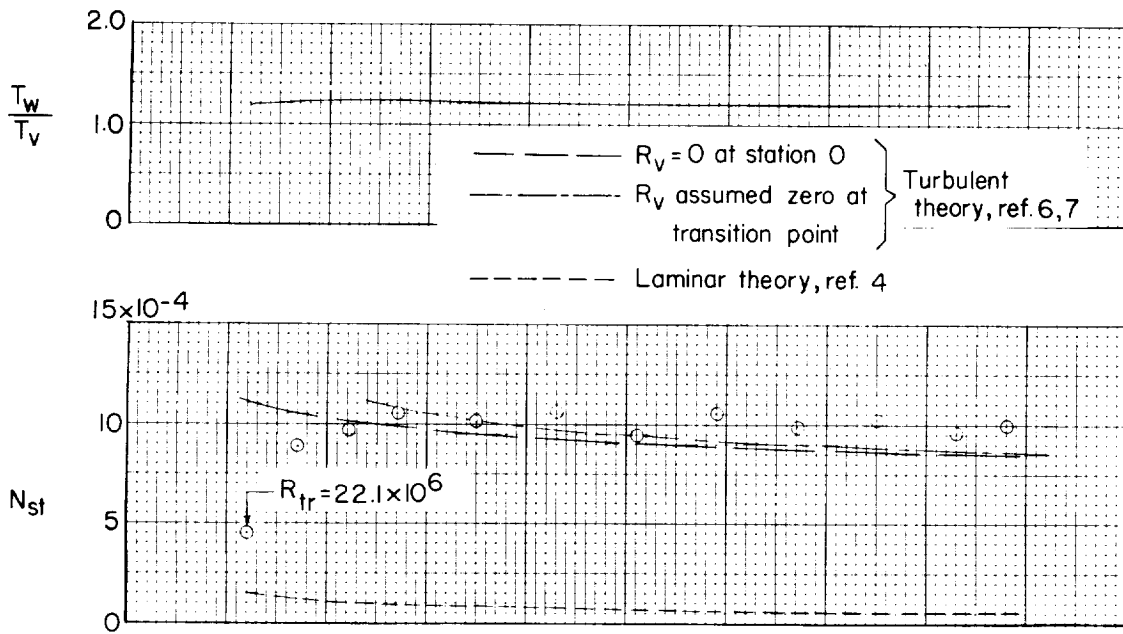


(a) 2.0 sec; $M_V = 1.96$; $R_V/ft = 13.6 \times 10^6$.

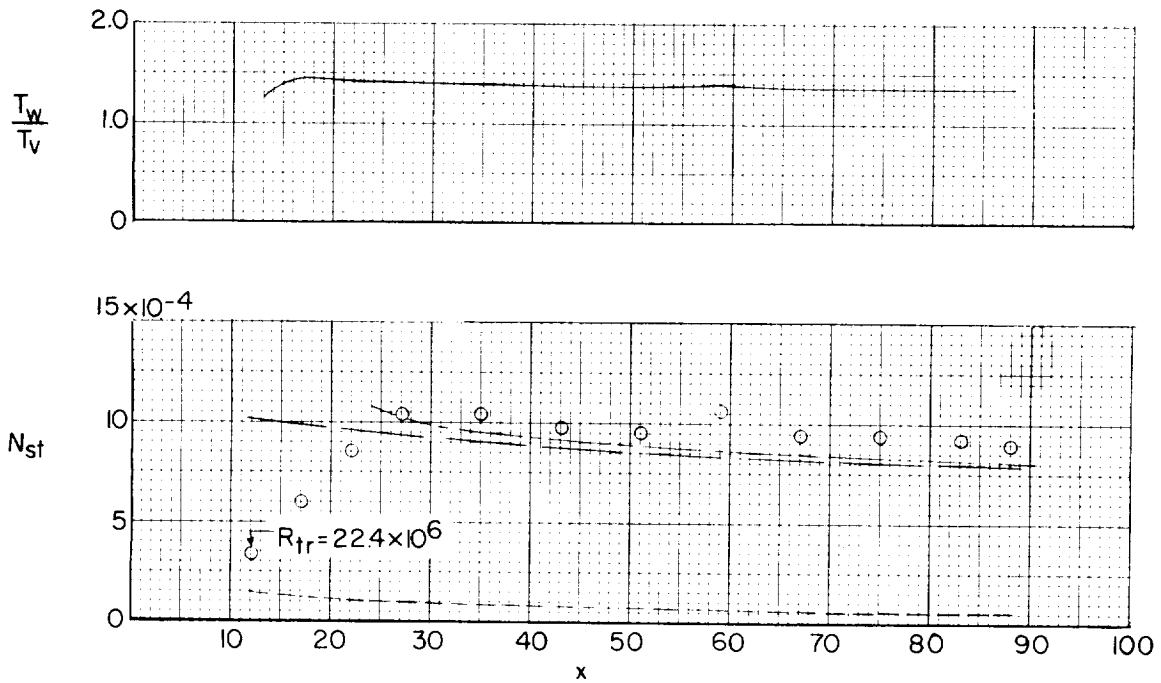


(b) 2.5 sec; $M_V = 2.64$; $R_V/ft = 18.2 \times 10^6$.

Figure 5.- The variation of Stanton number and wall temperature ratio with axial distance along body.

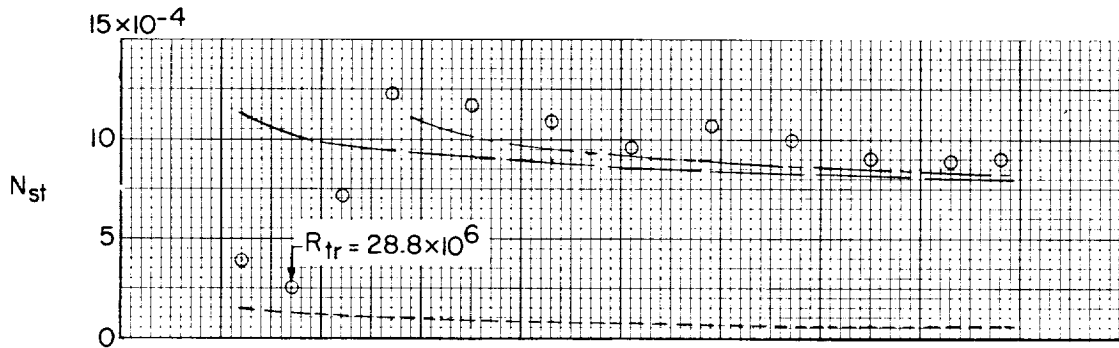
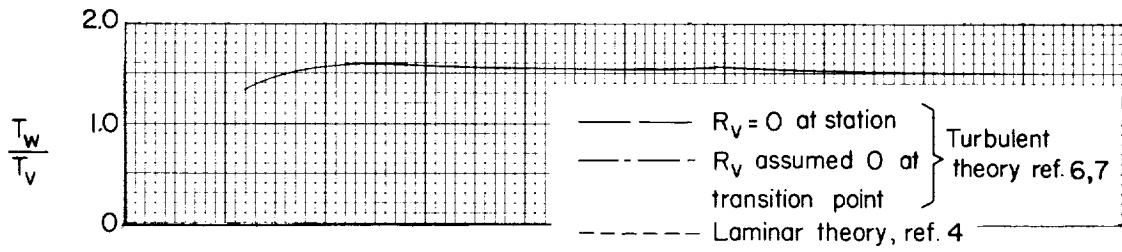


(c) 3.0 sec; $M_v = 3.28$; $R_v/ft = 22.1 \times 10^6$.

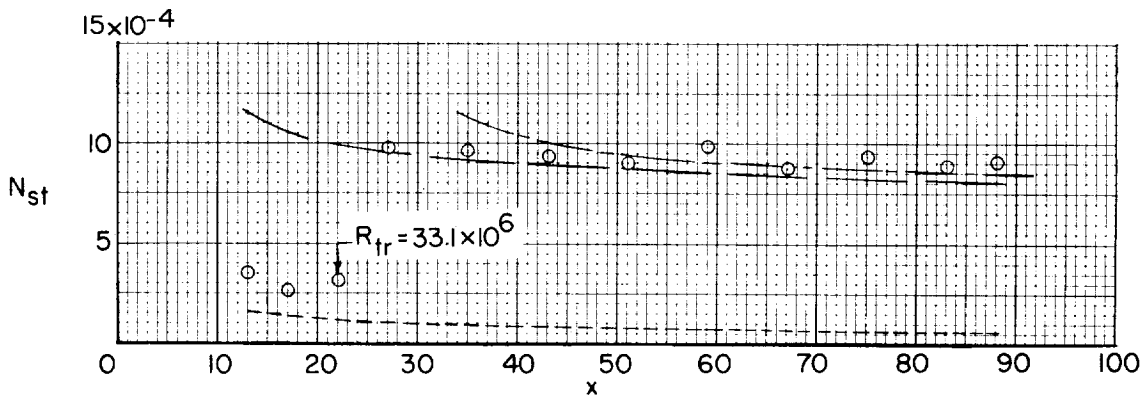
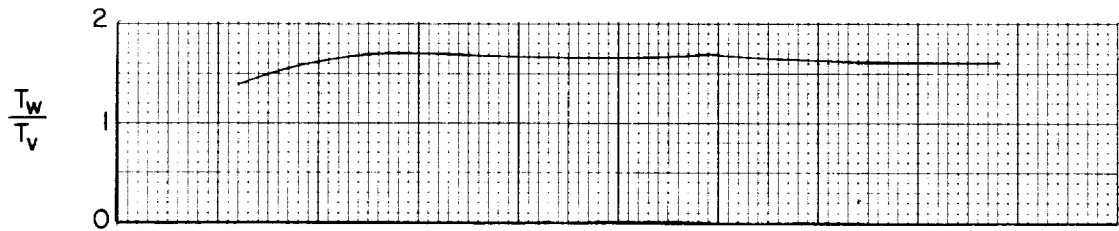


(d) 3.5 sec; $M_v = 3.48$; $R_v/ft = 22.4 \times 10^6$.

Figure 5.- Continued.



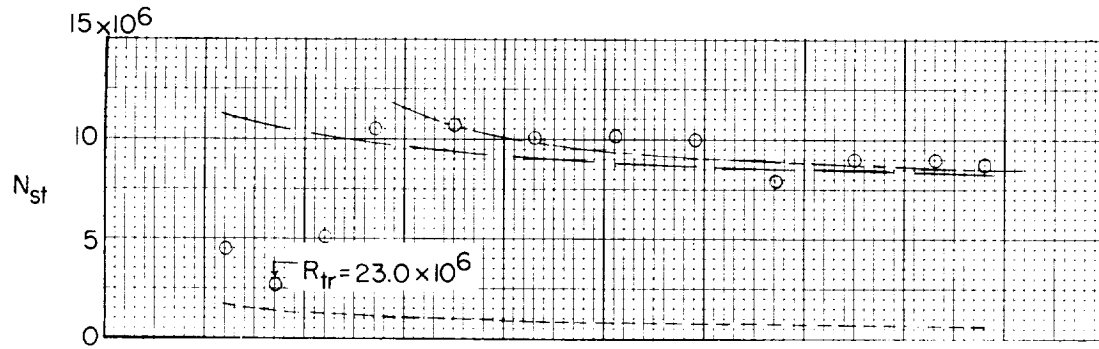
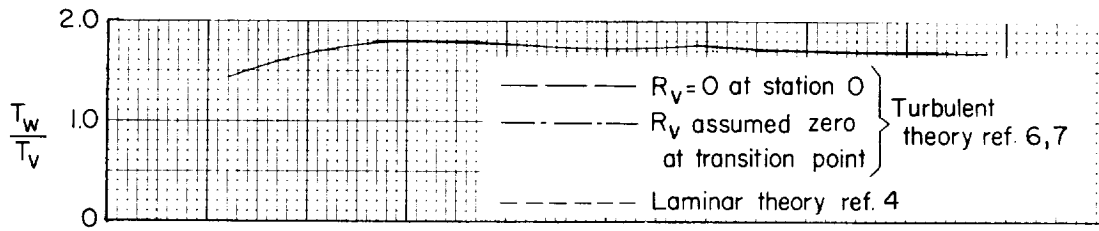
(e) 4.0 sec; $M_V = 3.31$; $R_V/ft = 20.2 \times 10^6$.



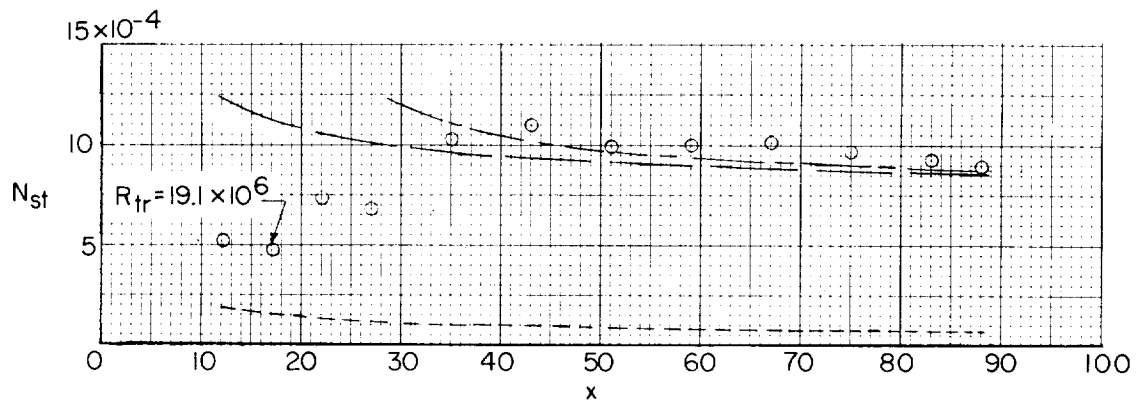
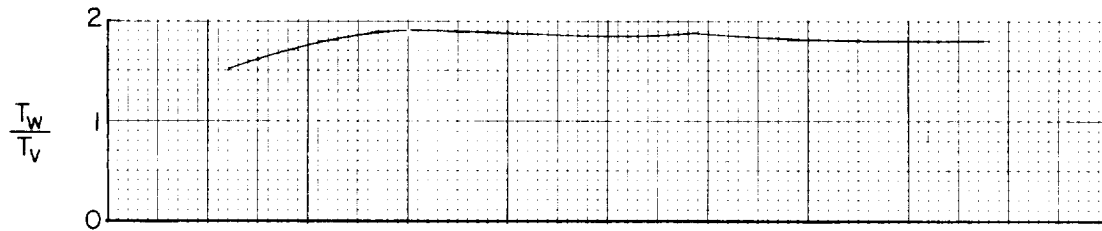
(f) 4.5 sec; $M_V = 3.15$; $R_V/ft = 18.1 \times 10^6$.

Figure 5.- Continued.

L-1700

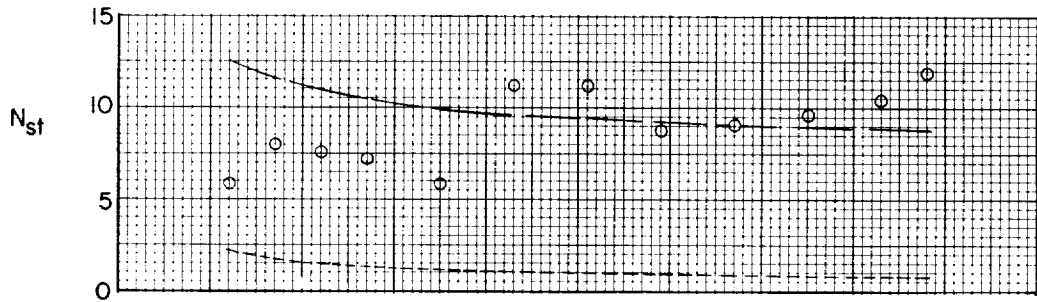
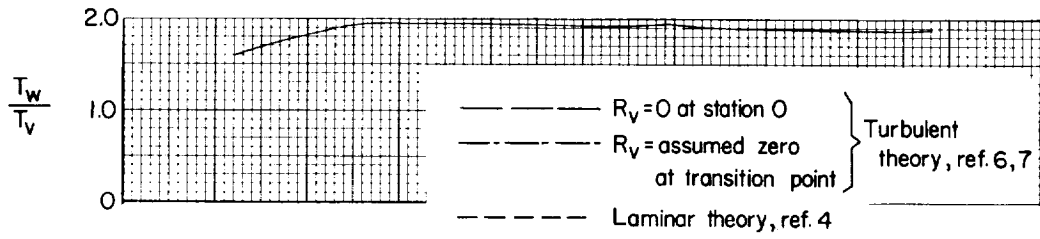


(g) 5.0 sec; $M_V = 3.01$; $R_V/ft = 16.3 \times 10^6$.

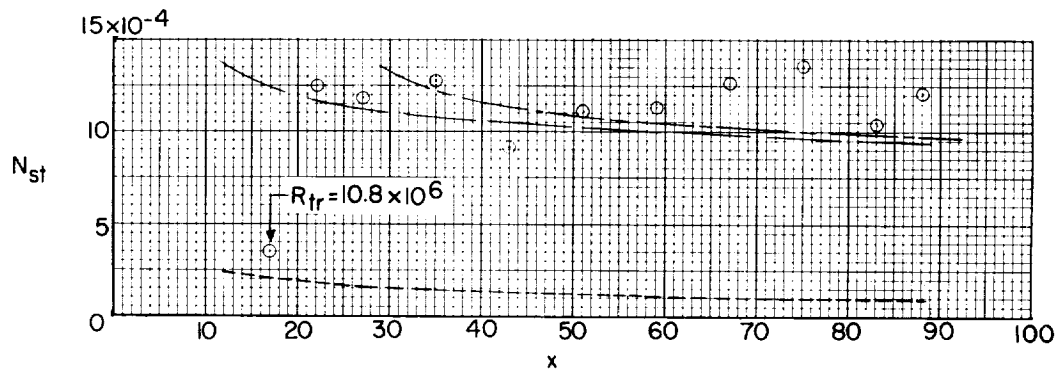
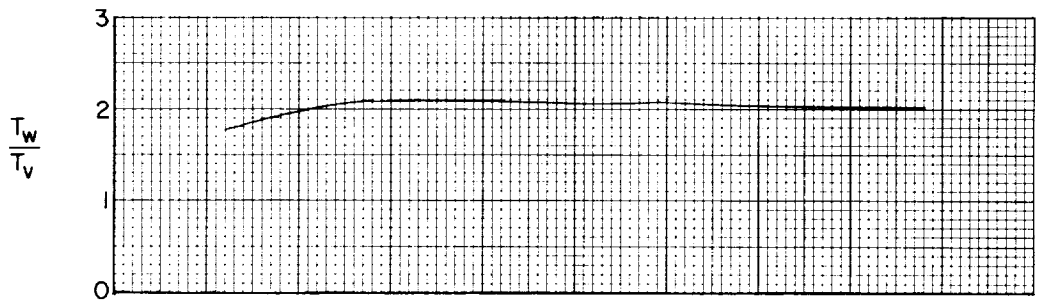


(h) 6.0 sec; $M_V = 2.78$; $R_V/ft = 13.5 \times 10^6$.

Figure 5.- Continued.

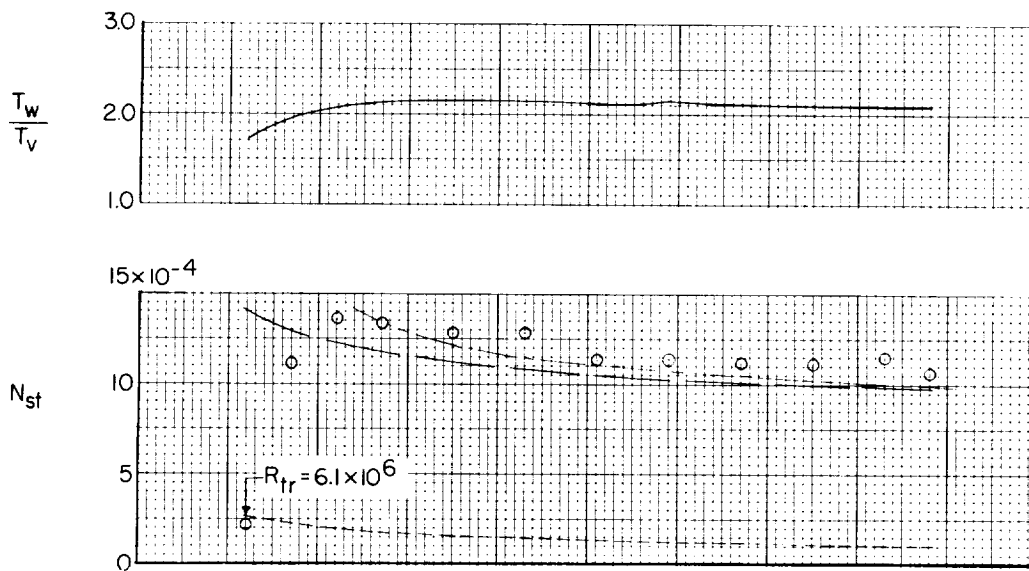


(i) 7.0 sec; $M_v = 2.58$; $R_v/ft = 11.3 \times 10^6$.

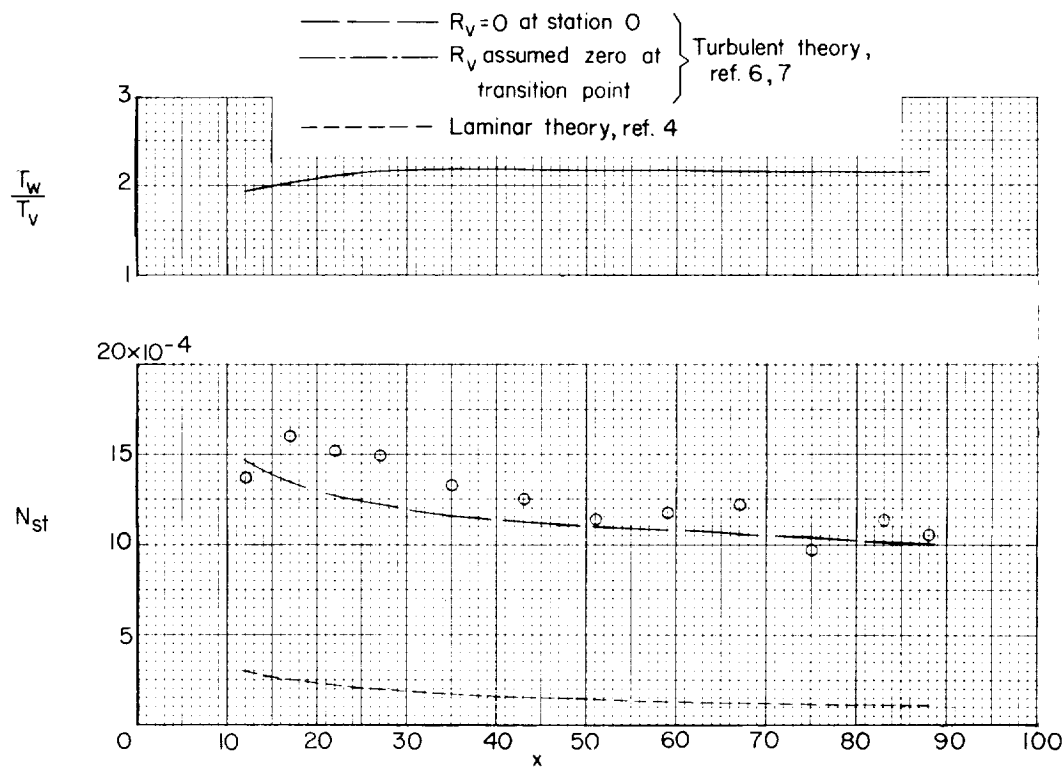


(j) 10.0 sec; $M_v = 2.17$; $R_v/ft = 7.6 \times 10^6$.

Figure 5.- Continued.



(k) 12.0 sec; $M_V = 1.96$; $R_V/ft = 6.1 \times 10^6$.



(l) 14.0 sec; $M_V = 1.79$; $R_V/ft = 5.0 \times 10^6$.

Figure 5.- Concluded.

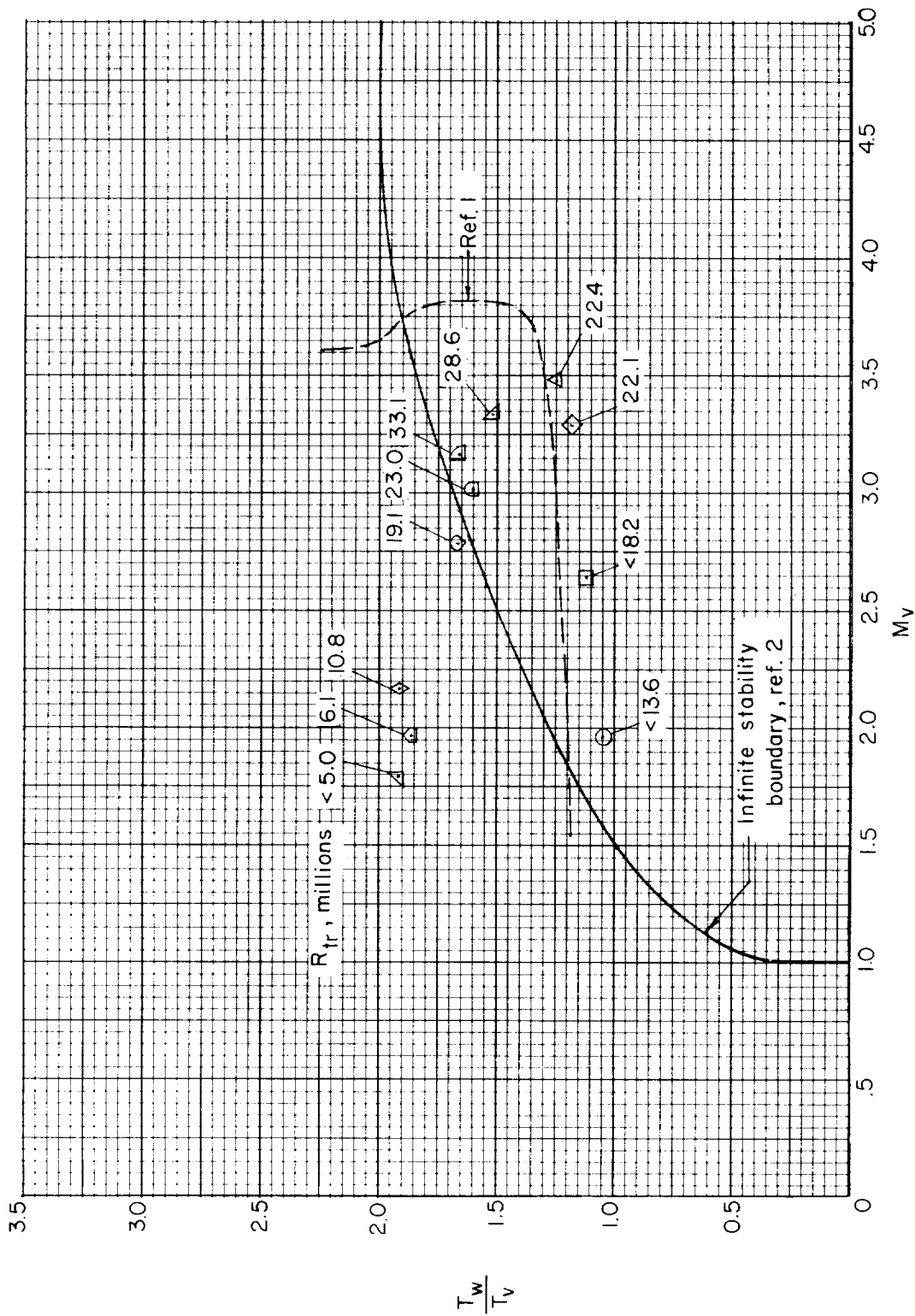


Figure 6.- Mach number and wall-temperature-ratio transition stations.

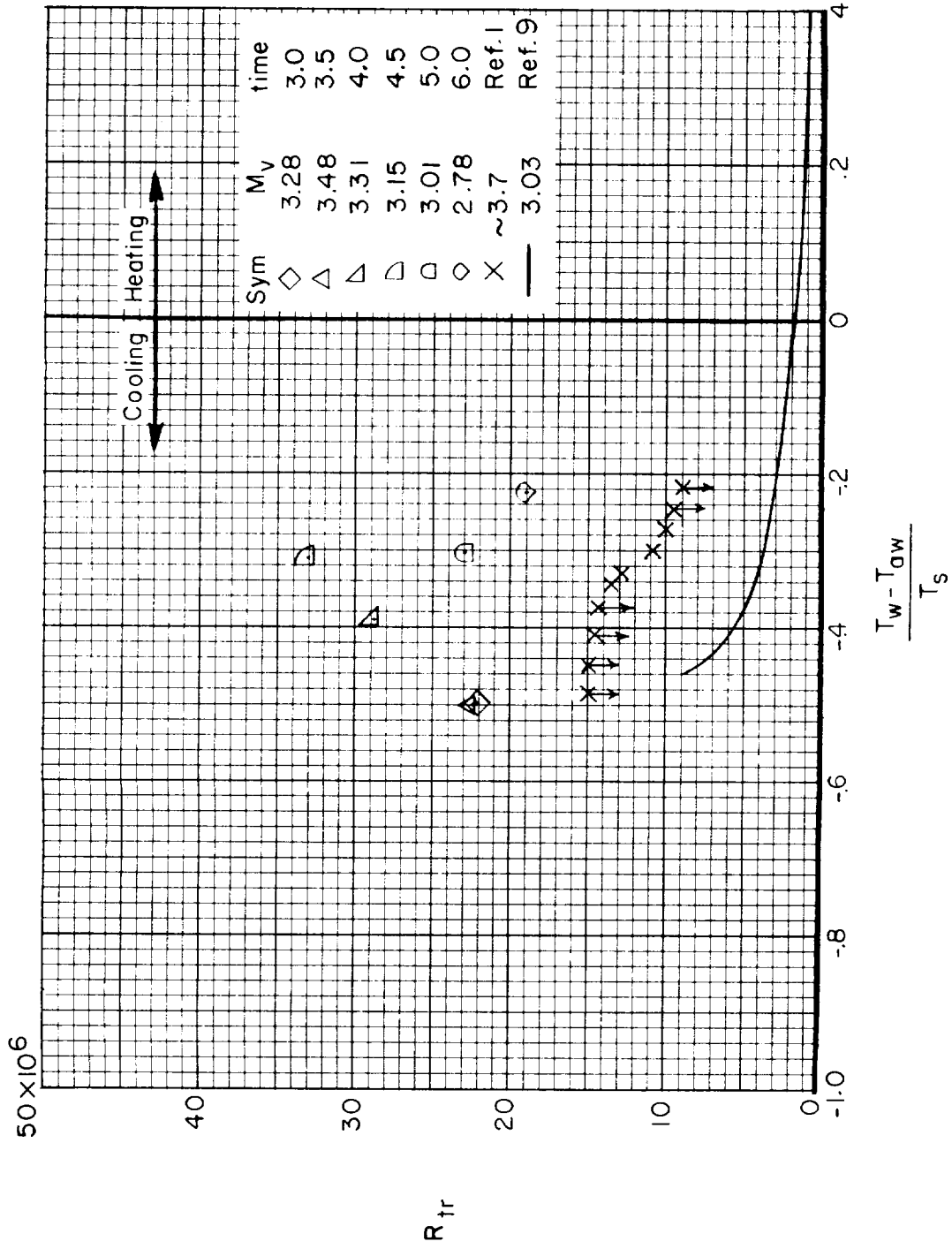


Figure 7.- Variation of transition Reynolds number with wall temperature parameter.

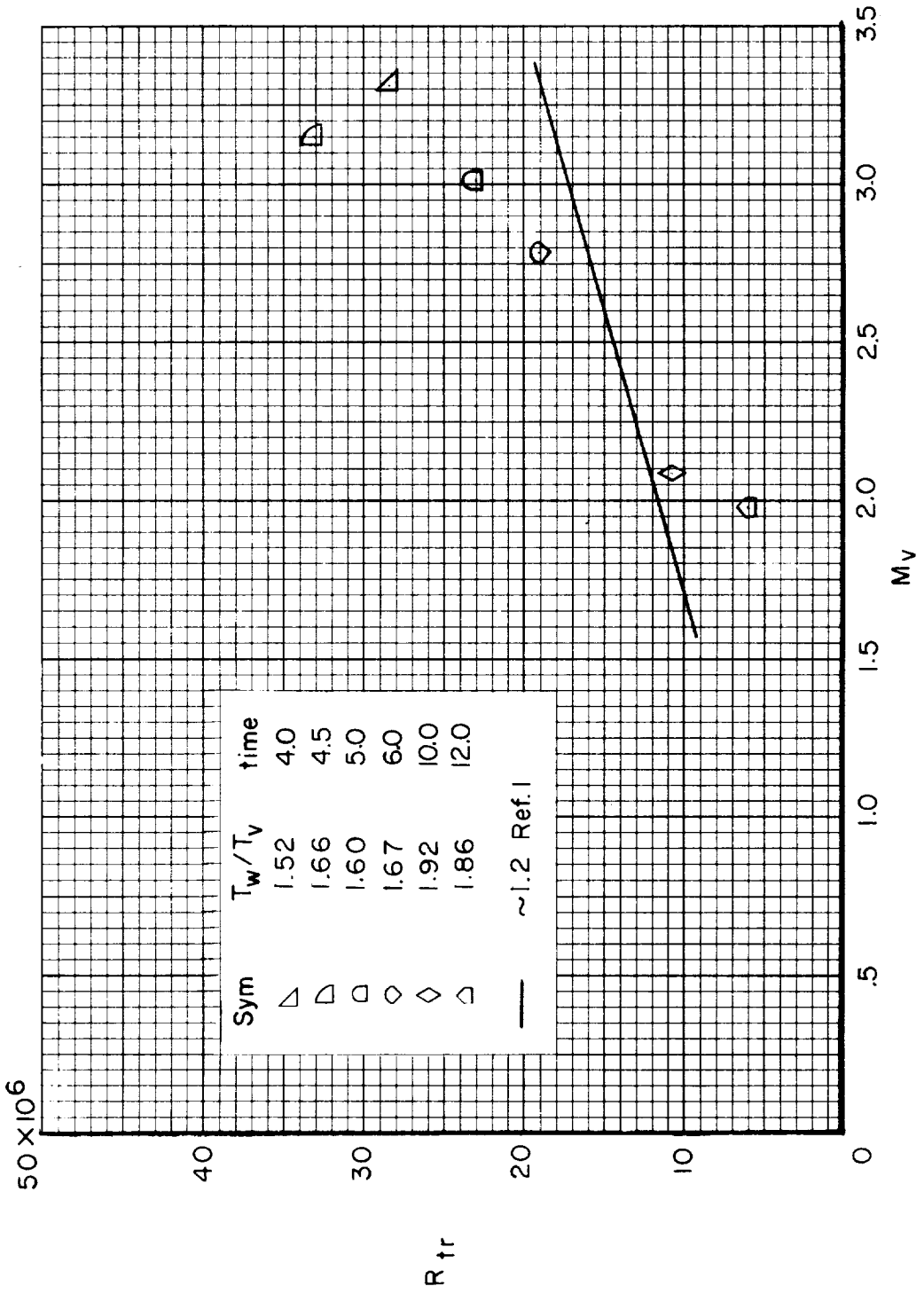


Figure 8.- Variation of transition Reynolds number with local Mach number.

•

4

•

•

•

•